Phase diagrams of epitaxial $Pb(Zr,Ti)O_3$ ultrathin films from first principles

David Sichuga,[1] I. Ponomareva,[2] and L. Bellaiche[1]
[1]*Physics Department, University of Arkansas, Fayetteville, Arkansas 72701, USA*
[2]*Department of Physics, University of South Florida, Tampa, Florida 33620, USA*
(Received 12 August 2009; revised manuscript received 29 September 2009; published 20 October 2009)

An *ab-initio-based* approach, that includes strain, ferroelectricity, and tilting of the oxygen octahedra as degrees of freedom, is developed to investigate *temperature-versus-misfit-strain* and *temperature-versus-composition* phase diagrams of $Pb(Zr,Ti)O_3$ ultrathin films near their morphotropic phase boundaries. Many features—originating from the interplay between composition, strain, polarization and oxygen octahedra tilting—are observed. Examples of such features are (i) an unusual behavior of the Curie temperature as a function of the compressive strain; (ii) a very rich variety of low symmetry phases; and (iii) several multiphase points that are each associated with four phases.

DOI: 10.1103/PhysRevB.80.134116 PACS number(s): 77.80.Bh, 68.55.−a, 77.55.+f, 77.84.Dy

I. INTRODUCTION

Ferroelectrics stand out among insulating solids because of their ability to maintain large reversible spontaneous polarization.[1] In addition, ferroelectric *solid solutions* can yield optimized properties, which make them widely used in a variety of devices. Of a particular interest are the $Pb(Zr_{1-x}Ti_x)O_3$ (PZT) solid solutions in a narrow compositional region centered around 50%. Such region is known as the morphotropic phase boundary (MPB), exhibits strong electromechanical couplings (as a result of the compositional-induced rotation of the polarization's direction),[2–4] and therefore finds numerous applications in piezoelectric actuators and transducers.[5] At the same time, the PZT systems remain an interesting object because of their relevance to miniaturization of devices, since recent experimental and theoretical results[6–12] explicitly revealed the dependence of properties of ferroelectric nanostructures on different specific factors. For instance, epitaxial ferroelectric films can exhibit structural phases that do not exist in the corresponding bulks because of the coupling between the strain arising from the substrate on top of which the films are grown and the polar displacements inside the films. In particular, the pioneering work of Pertsev *et al.*[13] established the relationship between the properties of single-crystalline PZT films and epitaxial strain conditions. More precisely, the used phenomenological approach allowed the construction of the temperature-versus-misfit-strain diagrams (known as Pertsev diagrams) in PZT thin films under short-circuit (SC) electrical boundary conditions, and revealed the existence of four stable phases depending on the strain-temperature combination imposed on PZT thin films. These Pertsev diagrams are readily accepted as useful tools for interpreting the observed properties of epitaxially grown PZT films. However, they correspond to rather thick films, implying that they are not technically valid for ultrathin films (where surprises may be in store due to the increasing role of surface effects). Moreover and even more importantly in our minds, they do not take in consideration the influence of a specific structural phenomenon—that strongly interacts with both the polarization and the strain in several ferroelectrics[14–17] and that is known to occur in *PZT bulks at low temperature* (see Refs. 18 and 19 and references therein)—on physical properties of PZT thin films. Such a phenomenon is the oxygen octahedra tilting—which is also denoted as *antiferrodistortive* (AFD) motions—and may thus be an important factor in structural transitions of PZT thin films in certain temperature-strain ranges.

The aim of this article is to reveal phase diagrams of PZT *ultrathin films* by developing and using an *ab initio* approach that incorporates the possibility of oxygen octahedra tilting, and its couplings with strain and polarization, for Ti compositions lying near the MPB area. Our main findings are that such tilting and its couplings give rise to *previously overlooked and important phenomena* in the Pertsev diagrams, such as (i) the existence of many phases; (ii) an unusual behavior of the Curie temperature versus the magnitude of the compressive strain; and (iii) the occurrence of several multiphase points where four phases meet. Furthermore, studying the *temperature-versus-composition* phase diagram for a given misfit strain also leads to an observance of many bridging, low-symmetry (e.g., triclinic) phases that are characterized by a compositional-induced rotation of the polarization and/or axis about which the oxygen octahedra tilt—because of the highly sensitive interplay between composition, strain, polarization, and oxygen octahedra's tilting in PZT thin films around their MPB.

The paper is organized as follows. Section II describes the first-principles-based approach developed in this work. Section III reports and discusses various predictions arising from the use of this approach, while Sec. IV provides some conclusions.

II. METHOD

In our simulations, we model epitaxial (001) films made of disordered $Pb(Zr_{1-x}Ti_x)O_3$ solid solutions by using $12\times12\times m$ supercells that are periodic along the x and y axes (chosen to lie along the pseudocubic [100] and [010] directions, respectively) and where m stands for the number of BO_2 layers along the *nonperiodic* z axis (chosen to be along the [001] pseudocubic direction)—where B atoms are either Zr or Ti. The complexity of the physical picture in the

 ©2009 The American Physical Society

real system is mirrored by the presently proposed expression for the total energy of the above supercell

$$E_{\mathrm{tot}}(\{\mathbf{u}_i\},\{\mathbf{v}_i\},\{\eta_{\mathrm{H}}\},\{\boldsymbol{\omega}_i\},\{\sigma_j\}) = E_{\mathrm{Heff}}(\{\mathbf{u}_i\},\{\mathbf{v}_i\},\{\eta_{\mathrm{H}}\},\{\boldsymbol{\omega}_i\},\{\sigma_j\}) + (\beta/2)\Sigma_i\langle E_{\mathrm{dep}}\rangle \cdot Z^*\mathbf{u}_i, \quad (1)$$

where the variable $\boldsymbol{u}_i$ is the local soft mode in unit cell i (which is directly proportional to the electric dipoles in the cell i),[20] $\boldsymbol{v}_i$ are inhomogeneous strain-related variables, and η_{H} is the homogeneous strain tensor.[20] $\boldsymbol{\omega}_i$ denotes a pseudovector centered at the B-site i that quantifies the direction and magnitude of AFD motions in the unit cell i. For instance, $\boldsymbol{\omega}_i=0.1\boldsymbol{z}$ corresponds to a rotation of the oxygen octahedra of cell i by *0.1* radians about the z axis—when denoting $\boldsymbol{z}$ as the unit vector along the z axis. Finally, $\sigma_j=+1$ (respectively, -1) characterizes the presence of a Zr (respectively, Ti) atom at the site j of the supercell. The total energy thus contains *all* the degrees of freedom responsible for the phase transitions of bulk PZT (i.e., it also includes the AFD motions, unlike Ref. 13). E_{Heff} is an (effective Hamiltonian) energy and consists of two terms

$$E_{\mathrm{Heff}}(\{\mathbf{u}_i\},\{\mathbf{v}_i\},\{\eta_{\mathrm{H}}\},\{\boldsymbol{\omega}_i\},\{\sigma_j\}) = E_{\mathrm{FE}}(\{\mathbf{u}_i\},\{\mathbf{v}_i\},\{\eta_{\mathrm{H}}\},\{\sigma_j\}) + E_{\mathrm{AFD}}(\{\mathbf{u}_i\},\{\mathbf{v}_i\},\{\eta_{\mathrm{H}}\},(\boldsymbol{\omega}_i),\{\sigma_j\}), \quad (2)$$

where E_{FE} is the energy associated with the ferroelectric and strain degrees of freedom, as well as their mutual couplings. Its analytical expression is the one indicated in Ref. 4 for bulk PZT, except for the long-range dipole-dipole interactions for which we use here the corresponding interactions for thin films under open-circuit (OC) electrical boundary conditions[21] rather than the ones of the bulk. As detailed in Refs. 4 and 20, the parameters of E_{FE} are determined by performing first-principle computations[22,23] on supercells containing up to 40 atoms. The second term of Eq. (2) accounts for the AFD distortions and their couplings with strain and electric dipoles. Its expression has been recently proposed in Ref. 18 and is given by

$$\begin{aligned} E_{\mathrm{AFD}}(\{\mathbf{u}_i\},\{\mathbf{v}_i\},\{\eta_{\mathrm{H}}\},\{\boldsymbol{\omega}_i\},\{\sigma_j\}) &= \Sigma_i[k_A\omega_i^2 + \alpha_A\omega_i^4 + \gamma_A(\omega_{i,x}^2\omega_{i,y}^2 + \omega_{i,y}^2\omega_{i,z}^2 + \omega_{i,x}^2\omega_{i,z}^2)] \\ &+ \Sigma_{i,j}\Sigma_{\alpha,\beta}K_{ij,\alpha\beta}\omega_{i,\alpha}\omega_{j,\beta} + \Sigma_i\Sigma_{\alpha,\beta,l}C_{l,\alpha\beta}\eta_l(i)\omega_{i,\alpha}\omega_{i,\beta} \\ &+ \Sigma_i\Sigma_{\alpha,\beta,\gamma,\delta}D_{\alpha\beta\gamma\delta}\omega_{i,\alpha}\omega_{i,\beta}u_{i,\gamma}u_{i,\delta} \\ &+ \Sigma_i\omega_i[A_0\sigma_i + \Sigma_jA_1\sigma_j]. \end{aligned} \quad (3)$$

Here, the summations over i run through all the B sites, while the sums over j run over the six nearest B neighbors of a given B site. The components of the total strain (that is, that contain both homogenous and inhomogeneous parts) at the site i are denoted as $\eta_l(i)$, in Voigt notation, and the Cartesian components α, β, γ, and δ are given along the x, y, and z axis that coincide with the crystallographic [100], [010], and [001] directions, respectively. The first four energetic terms of Eq. (3) are the self-energy associated with AFD motions, the short-range interaction energy between AFD degrees of freedom, the interaction energy between strain and $\boldsymbol{\omega}_i$, and the interaction energy between local modes and AFD motions, respectively. The last term in Eq. (3) represents how the actual atomic distribution in the PZT system affects the AFD motions, and thus takes into account the alloying effects. The parameters k_A, α_A, γ_A, $K_{ij,\alpha\beta}$, $C_{l,\alpha\beta}$, and $D_{\alpha\beta\gamma\delta}$ have been determined by performing calculations within the *local-density-approximation* (LDA) and the *virtual crystal approximation*[22,23] on *10-atom* supercells (i.e., supercells for which the B atom is a virtual atom made by computationally mixing a Ti and a Zr atom),[22] while the A_0 and A_1 parameters are found from LDA calculations on supercells containing *real* Zr and Ti atoms.

The second term of Eq. (1) represents the depolarizing energy and is computed according to Refs. 21 and 24, where $Z^*\boldsymbol{u}_i$ is the local electric dipole in unit cell i (Z^* being a Born effective charge).[20] It involves the screening parameter β that controls the magnitude of the depolarizing field $\langle \boldsymbol{E}_{\mathrm{dep}}\rangle$ in the following way: $\beta=0$ corresponds to ideal OC electrical boundary conditions (maximum magnitude of the depolarizing field), $\beta=1$ corresponds to ideal SC electrical boundary conditions (no depolarizing field), and a value of β in-between corresponds to more realistic cases for which a residual (nonzero and nonmaximum) depolarizing field exists. Also note that, as in Refs. 21 and 24, our total energy, E_{tot}, assumes a simple truncation, at the surface/interface layers, of the interactions existing in bulk PZT.

Mechanical boundary conditions consistent with an epitaxial growth of (001) films are also mimicked by freezing some components of the homogeneous strain tensor, namely (in Voigt notation), $\eta_{\mathrm{H},6}=0$ and $\eta_{\mathrm{H},1}=\eta_{\mathrm{H},2}=\delta$. The latter represents the misfit strain between the film and the substrate[25,26] and is defined as $\delta=(a_{\mathrm{sub}}/a_{\mathrm{ref}})-1$, where a_{sub} is the in-plane lattice constant of the substrate and where $a_{\mathrm{ref}}=4.04$ Å is the lattice constant of the PZT bulk (for a Ti composition of 50%) at its cubic-to-tetragonal transition. $\delta>0$ or $\delta<0$ characterizes the type of the in-plane strain experienced by the epitaxial film, that is, tensile or compressive, respectively.

The above total energy of Eq. (1) is used in Monte Carlo (MC) simulations—with 4×10^4 MC sweeps and starting from high temperature and then decreasing the temperature in small steps—to compute finite-temperature properties of (001) epitaxial PZT films. The results discussed below correspond to the use of $12\times12\times12$ supercells and $\beta=0.98$ since such latter value has been found to yield good agreement with (unpublished) experiments on various nanostructures. Statistical averages (over the MC sweeps) of different physical quantities were computed at each temperature. For instance, we were interested in obtaining the $\langle \boldsymbol{u}\rangle$ supercell average of the local mode vectors $\boldsymbol{u}_i$, which is directly proportional to the polarization. The analysis of its evolution allowed us to identify the ferroelectric phase transitions. Another quantity of interest used to identify phase transitions associated with the tilting of the oxygen octahedra is the supercell average vector $\langle \boldsymbol{\omega}\rangle_{\mathrm{R}}$, which is defined[18] as $\langle \boldsymbol{\omega}\rangle_{\mathrm{R}} = (1/N)\Sigma_i\boldsymbol{\omega}_i(-1)^{nx(i)+ny(i)+nz(i)}$, where the sum runs over the N sites i and where nx(i), ny(i), and nz(i) are integers associated with the location of the cell i inside the supercell (i.e., the B site i is centered around $[nx(i)\boldsymbol{x}+ny(i)\boldsymbol{y}+nz(i)\boldsymbol{z}]a$,

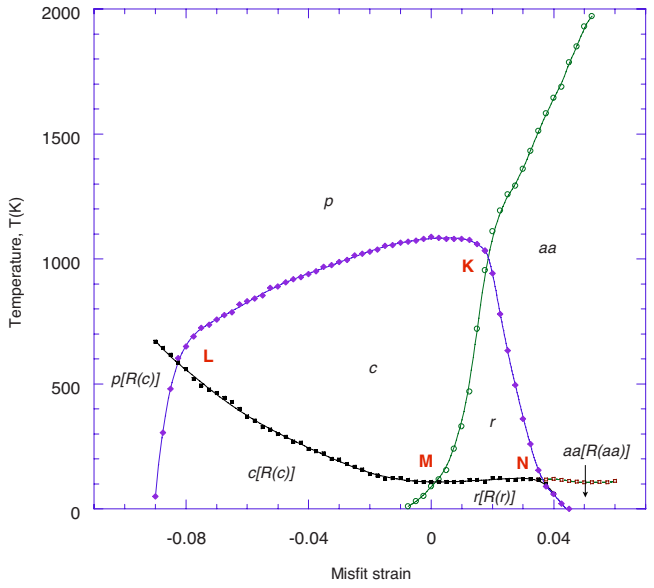

FIG. 1. (Color online) Temperature-versus-misfit-strain phase diagram of a $Pb(Zr_{0.52}Ti_{0.48})O_3$ ultrathin film of 48 Å thickness and under short-circuit-like conditions (namely, β=0.98). *K*, *L*, *M*, and *N* indicate multiphase points where four phases meet, while the notations explained in the text for the different phases are used here.

where a is the $(0\ K)$ cubic-lattice constant of PZT and where $\boldsymbol{x}$, $\boldsymbol{y}$, and $\boldsymbol{z}$ are unit vectors along the Cartesian axes). A nonvanishing $\langle \boldsymbol{u} \rangle$ indicates the existence of ferroelectricity while a nonzero $\langle \boldsymbol{\omega} \rangle_R$ characterizes the appearance of AFD motions associated with the *R* point of the cubic first Brillouin zone. Note that, for all the calculations we performed during this present study, summing $\boldsymbol{\omega}_i$ over all the sites i was found to yield the zero vector, and that we did not find any phase corresponding to the appearance of AFD motions associated with the *M* point of the cubic first Brillouin zone.

III. RESULTS

Figure 1 displays the predicted temperature-versus-misfit-strain phase diagram for a $Pb(Zr_{0.52}Ti_{0.48})O_3$ ultrathin film having a thickness of 48 Å (as modeled by a $12\times12\times12$ supercell) under *almost ideal* SC conditions (namely, β =0.98). We chose here a Ti composition of 48% because it lies in the heart of the MPB area in the bulk,[18] and is thus of large technological importance. (Note that some calculations were done for very high, and thus unrealistic, values of the epitaxial strain, in order to have a complete qualitative picture of the possible phases involved in the Pertsev phase diagrams. However, we numerically found that one can change some physical parameters inherent to films, such as the screening parameter and thickness, to make the phases of Fig. 1 appearing in a more realistic strain range.) One can first notice a multiphase point, denoted by *K*, where four stable phases "meet" each other. These phases are known to originate from the coupling between the epitaxial strain and the polarization[13] and are (following the notation of Ref. 13): the *p* (paraelectric) phase; the *c* state, that is of tetragonal symmetry, that occurs for large compressive strain and for which the polarization lies along the out-of-plane [001] direction; the *aa* phase, which is of orthorhombic symmetry, that occurs for large tensile strain, and for which the polarization is aligned along the in-plane [110] direction; and the *r* state, that is of monoclinic symmetry (rather than rhombohedral as its notation may wrongly imply), and which can be considered as a bridge between the *c* and *aa* states because its polarization continuously rotates from the [001] to [110] directions as the strain increases from intermediate negative values to intermediate positive values. As a result, in the nearest vicinity of the multiphase point *K*, our diagram resembles the one of Ref. 13, although our crosspoint *K* is shifted away from the zero misfit strain—resulting in the expansion of the *c* phase into the region of positive strains. The root of this displacement of the *K* point resides in a surface-induced enhancement of the z component of polarization, and is thus a feature of *ultrathin* films.[26] Moreover, several striking features appear in our Fig. 1, were missed in Ref. 13 and lead to a revisiting of the predictions of Ref. 13, mostly because they involve tilting of oxygen octahedra (an important physical property not included in the approach used by Ref. 13). For instance, at low temperature and largest investigated compressive strain, a new phase is predicted to occur. Such phase is paraelectric, is solely characterized by the oxygen octahedra tilting about the *out-of-plane* direction, and adopts a tetragonal symmetry. We denote such phase as $p[R(c)]$, by generalizing the Pertsev's notations[13] in the following manner: (i) what is inside the brackets refers to the tilting of the oxygen octahedra with the "*R*" letter emphasizing that the condensation of these AFD modes occurs at the *R* point of the cubic first Brillouin zone; (ii) the symbol inside the parentheses (that are themselves inside the brackets) provides information about the axis about which the oxygen octahedra tilt, in the same manner that this symbol characterizes the direction of the polarization in the Pertsev's phases (i.e., "(c)" inside the brackets means that the tilt is about the z axis); (iii) the letter(s) on the left side of the brackets refers to the polarization as in the Perstev's notation (i.e, "*p*" means that there is no polarization). Furthermore, three other (previously overlooked) phases, that all exhibit coexistence between FE and AFD motions, are found at low temperature. They are: the tetragonal $c[R(c)]$ state that occurs for relatively large compressive strain and for which the direction of the polarization and the axis about which the oxygen octahedra tilt are both along the out-of-plane [001] direction; the orthorhombic $aa[R(aa)]$ state that occurs for large tensile strain and for which the direction of the polarization and the axis about which the oxygen octahedra tilt are both along the in-plane [110] direction; and the monoclinic $r[R(r)]$ phase that is stable for intermediate misfit strains and for which the polarization aligns along a $[uuv]$ direction while the oxygen octahedra tilt about an $[u'u'v']$ direction (with u and u', as well as v and v', being not necessarily equal to each other). Interestingly, this $r[R(r)]$ phase can also be considered as a bridging structure in the sense that both the polarization and the axis about which the oxygen octahedra tilt continuously rotate from a [001] to [110] direction as the strain increases. The $c[R(c)]$, $aa[R(aa)]$, and $r[R(r)]$

phases originate from the facts that (i) *bulk* $Pb(Zr_{0.52}Ti_{0.48})O_3$ exhibits a low-temperature (Cc) phase in which polarization and tilting of oxygen octahedra coexist,[18] and (ii) that FE and AFD degrees of freedom not only individually couple with strain but also couple with each other, favoring a tilting of the oxygen octahedra about a direction equal or close (in case of monoclinic states) to the strain-induced direction of the polarization. Such various, simultaneous couplings give rise to several features. One example is the existence of three multiphase points that are each associated with four phases and that are denoted by *L*, *M*, and *N* in Fig. 1. [The phase diagram of Fig. 1 thus predicts the existence of eight phases with four multiphase points, unlike Ref. 13.] Another striking example is the fact that the transition (Curie) temperature between the *p* and *c* states strongly *decreases* as the compressive strain increases in magnitude. Such behavior happens because increasing the strength of the compressive strain strongly enhances AFD motions (as also found in Ref. 27 for pure $SrTiO_3$ and as one can see by, e.g., looking at the strain-induced increase of the *c*-to-$c[R(c)]$ transition temperature in Fig. 1), while it only slightly directly affects the polarization in PZT systems,[24,28] and because the AFD and FE motions compete against each other in PZT materials.[18] The fact that the *p*-to-*c* (Curie) transition temperature decreases (from around 1000 to 0 K) as the compressive strain increases is completely opposite to what occurs in films made of "classical" materials (such as $BaTiO_3$ films) that do not exhibit any AFD motions,[25,26,29,30] and has never been reported to the best of our knowledge. It is also of huge technological interest because it implies that many properties (such as dielectric and piezoelectric responses) can be optimized for *any* temperature below 1000 K, by choosing the right substrate—since such properties are known to peak at the Curie temperature.

The "topology" of the phase diagram depicted in Fig. 1 can be changed by varying the screening parameter β and/or the thickness of the film. This dependence (not shown here) is straightforward to understand in the light of the above discussion. Indeed, a decrease in the value of the β parameter, for instance, leads to a larger depolarizing field in the sample and, therefore, to a smaller *z* component of the polarization (below the Curie temperature). As a result, (1) the *c*-to-*p* transition temperatures drop and the multiphase *K* point shifts toward lower temperature and closer to the zero-strain line on the diagram, and (2) the *c*-to-$c[R(c)]$ transition line elevates from its previous position, indicating the increase in temperatures at which the oxygen octahedra distortion takes place. Similarly, increasing the thickness for the given β value has the same qualitative trends (1) and (2) described above, because such increase minimizes the effect of the surface-induced enhancement of the *z* component of the dipoles on physical properties and thus leads to a smaller *z* component of the (average) polarization—since the ratio of inner layers over surface layers increases as the thickness increases.

Let us now investigate the *temperature-versus-Ti composition* phase diagram for a constant misfit strain. We chose here a value of +2.5% for that misfit strain because it lies at the heart of the "bridging" *r* and $r[R(r)]$ phases in Fig. 1. Such a diagram is shown in Fig. 2 for Ti compositions lying inside or near the MPB area. One can indeed clearly see the existence of 12 phases that were absent in Fig. 1 and that have never been reported in PZT films to the best of our knowledge. Such states are (i) four purely ferroelectric states: the orthorhombic *a* phase (for which the polarization lies along the pseudocubic [100] direction), the monoclinic *ab* phase (for which the polarization is along an in-plane $[uv0]$ direction, with *u* different from *v*), the monoclinic *ac* phase (for which the polarization is parallel to a $[u0w]$ direction, with *u* different from *w*), and the triclinic *abc* phase (for which the polarization lies along a $[uvw]$ direction, with *u*, *v*, and *w* all different from each other and nonzero); and (ii) eight phases exhibiting a coexistence between FE and AFD degrees of freedom at low temperature: the triclinic $abc[R(abc)]$, $abc[R(ab)]$, *and* $abc[R(a)]$ states (for which the oxygen octahedra tilt about a $[uvw]$, $[uv0]$, and a [100] direction, respectively); the triclinic $ac[R(abc)]$, and $ac[R(ab)]$ states; the monoclinic $ac[R(a)]$ and $a[R(ab)]$ states; and the orthorhombic $a[R(a)]$ state, for which the direction of the polarization and the axis about which the oxygen octahedra tilt are along the pseudocubic [100] direction. Such a variety of phases lead to nine points where four phases meet (as indicated by the letters *K* to *S*, in Fig. 2), and are bridging structures in the sense that they allow a continuous rotation of the polarization's direction and/or the axis about which the oxygen octahedra tilt, as the Ti concentration varies in the MPB area. Such a continuity is evidenced by, e.g., the $r-abc-ac-a$ ferroelectric phase transitions sequence occurring at 300 K, and the $r[R(r)]-abc[R(abc)]-ac[R(abc)]-ac[R(ab)]-a[R(ab)]-a[R(a)]$ phase transitions sequence happening at the lowest temperatures as the Ti concentration increases from 48% to 58%. Continuous rotation of the FE and AFD degrees of freedom, as a function of composition, is also a feature of PZT bulk in its MPB area (see, e.g., Ref. 18 and references therein). However, the mutual couplings between polarization, oxygen octahedra tilting, and the strain inherent to epitaxial films lead to the occurrence of phases that are absent in the bulk. For instance, Ref. 18 never found any triclinic phase in the MPB area of PZT bulks. One should also emphasize that having low-symmetry phases (in which polarization rotates) is particularly important when realizing that such phases are usually associated with large piezoelectric and dielectric responses.[2–4]

IV. CONCLUSIONS

In summary, we developed and used a first-principles-based approach to determine phase diagrams of epitaxial PZT ultrathin films close to their morphotropic phase boundaries. Such calculations led to a revisit of the previously published Pertsev phase diagrams[13] by distinguishing phases and anomalous features (such as a decrease in the Curie temperature as the compressive strain increases in magnitude or the occurrence of several multiphase points that are each associated with four phases). All these phases and features originate from the incorporation of the oxygen octahedra tilting and its couplings with strain and electric dipoles in the calculations. We also revealed a very rich variety of "bridg-

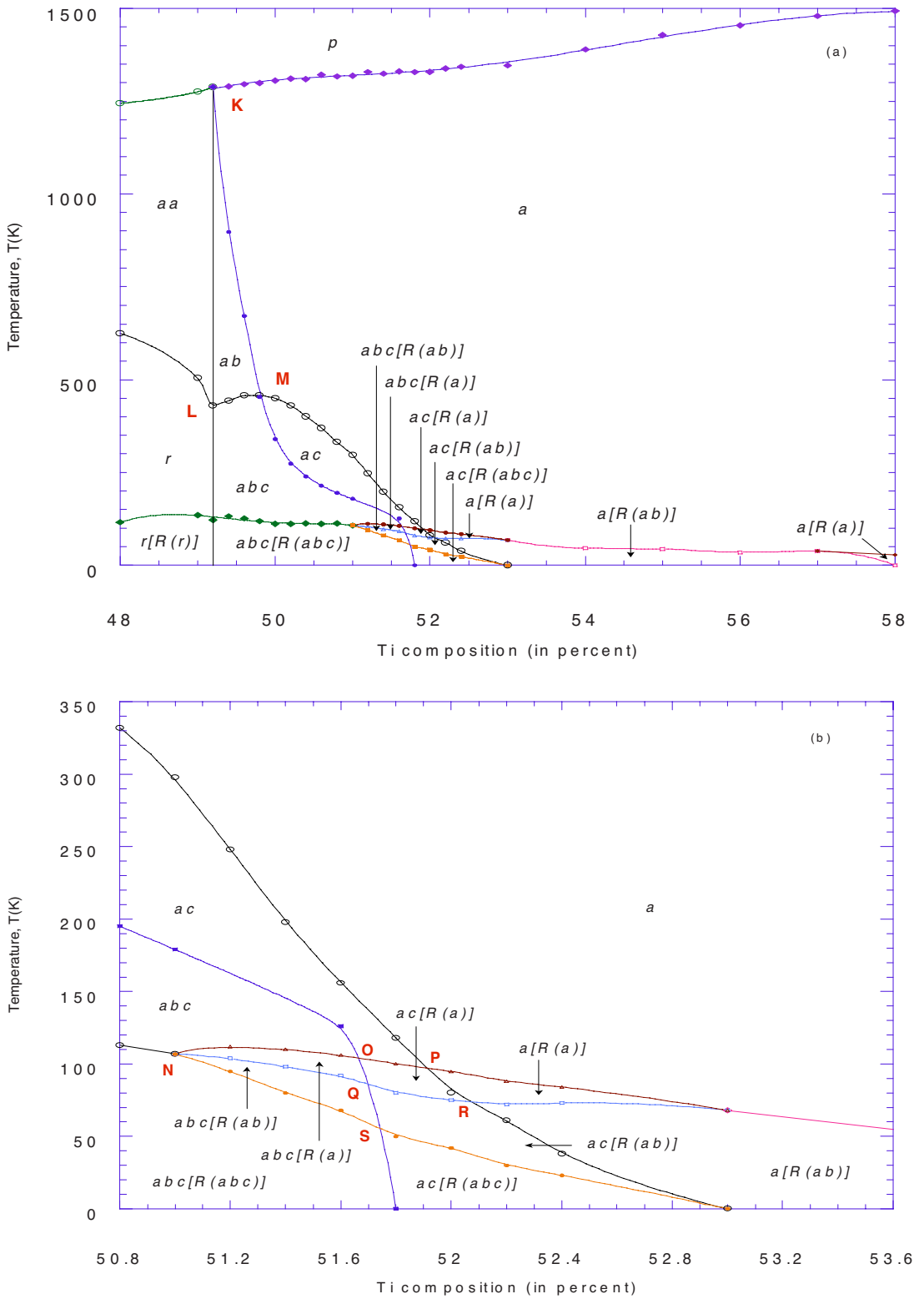

FIG. 2. (Color online) Temperature-versus-composition phase diagram of PZT ultrathin films having a 48 Å thickness and being under short-circuit-like conditions (namely, β=0.98) and a tensile epitaxial strain of +2.5%. Panel (b) shows an enlargement of the compositional region ranging between Ti concentrations of 50.8% and 53.6% and from a temperature up to 350K. *K*, *L*, *M*, *N*, *O*, *P*, *Q*, *R*, and *S* indicate multiphase points where four phases meet, while the notations explained in the text for the different phases are used here.

ing," low symmetry (e.g., triclinic) phases, depending on the composition and temperature for a given misfit strain. Such variety reflects the high sensitivity of the direction of polarization and of the axis about which the oxygen octahedra tilt on composition and strain. We hope that our predictions will be experimentally confirmed soon, and lead to a broader

knowledge of the fascinating fields of ferroelectric nanostructures and phase transitions. Note that our computations were all done for defect-free thin films, and that it may be interesting to investigate in the future the effect of defects on phase diagrams of ferroelectric nanostructures—especially when realizing that defects are already known to significantly affect properties of complex systems in their bulk forms (see, e.g., Ref. 31).

ACKNOWLEDGMENTS

This work is supported by ONR under Grants No. N00014-04-1-0413, No. N00014-08-1-0915, and No. N00014-07-1-0825 (DURIP), NSF under Grants No. DMR 0701558, No. DMR-0404335, No. DMR-0080054 (C-SPIN), and DOE under Grant DE-SC0002220. Some computations were made possible thanks to the MRI Grant No. 0722625 from NSF. We thank D. Vanderbilt for useful discussions.

[1] M. E. Lines and A. M. Glass, *Principles and Applications of Ferroelectrics and Related Materials* (Clarendon Press, Oxford, 1977).
[2] H. Fu and R. E. Cohen, Nature (London) **403**, 281 (2000).
[3] B. Noheda, D. E. Cox, G. Shirane, S. E. Park, L. E. Cross, and Z. Shong, Phys. Rev. Lett. **86**, 3891 (2001).
[4] L. Bellaiche, A. Garcia, and D. Vanderbilt, Phys. Rev. Lett. **84**, 5427 (2000); Ferroelectrics **266**, 41 (2002).
[5] K. Uchino, *Piezoelectric Actuators and Ultrasonic Motors* (Kluver Academic Publishers, Boston, 1996).
[6] T. M. Shaw, S. Trolier-McKinstry, and P. C. McIntyre, Annu. Rev. Mater. Sci. **30**, 263 (2000).
[7] Y. Drezner and S. Berger, J. Appl. Phys. **94**, 6774 (2003).
[8] B.-K. Lai, H. Kan, S. M. Phillips, and A. H. Heuer, Ferroelectrics **306**, 221 (2004).
[9] Y. Yoneda, T. Okabe, K. Sakaue, and H. Terauchi, J. Appl. Phys. **83**, 2458 (1998).
[10] I. Kornev, H. Fu, and L. Bellaiche, Phys. Rev. Lett. **93**, 196104 (2004).
[11] B. S. Kang, J.-G. Yoon, T. K. Song, S. Seo, and T. W. Noh, Jpn. J. Appl. Phys., Part 1 **41**, 5281 (2002).
[12] J. Junquera and P. Ghosez, Nature (London) **422**, 506 (2003).
[13] N. A. Pertsev, V. G. Kukhar, H. Kohlstedt, and R. Waser, Phys. Rev. B **67**, 054107 (2003).
[14] W. Zhong and D. Vanderbilt, Phys. Rev. B **53**, 5047 (1996).
[15] D. Vanderbilt and Z. Zhong, Ferroelectrics **206**, 181 (1998).
[16] D. J. Singh, Ferroelectrics **194**, 299 (1997).
[17] C.-H. Lin, C.-M. Huang, and G. Y. Guo, J. Appl. Phys. **100**, 084104 (2006).
[18] I. A. Kornev, L. Bellaiche, P.-E. Janolin, B. Dkhil, and E. Suard, Phys. Rev. Lett. **97**, 157601 (2006).
[19] M. Fornari and D. J. Singh, Phys. Rev. B **63**, 092101 (2001).
[20] W. Zhong, D. Vanderbilt, and K. M. Rabe, Phys. Rev. B **52**, 6301 (1995).
[21] I. Ponomareva, I. Naumov, I. Kornev, H. Fu, and L. Bellaiche, Phys. Rev. B **72**, 140102(R) (2005).
[22] L. Bellaiche and D. Vanderbilt, Phys. Rev. B **61**, 7877 (2000).
[23] P. Hohenberg and W. Kohn, Phys. Rev. **136**, B864 (1964); W. Kohn and L. J. Sham, *ibid.* **140**, A1133 (1965).
[24] S. Bin-Omran, I. Ponomareva, and L. Bellaiche, Phys. Rev. B **77**, 144105 (2008).
[25] O. Dieguez, S. Tinte, A. Antons, C. Bungaro, J. B. Neaton, K. M. Rabe, and D. Vanderbilt, Phys. Rev. B **69**, 212101 (2004).
[26] B.-K. Lai, I. A. Kornev, L. Bellaiche, and G. J. Salamo, Appl. Phys. Lett. **86**, 132904 (2005).
[27] N. A. Pertsev, A. K. Tagantsev, and N. Setter, Phys. Rev. B **61**, R825 (2000); **65**, 219901 (2002).
[28] H. N. Lee, S. M. Nakhmanson, M. F. Chisholm, H. M. Christen, K. M. Rabe, and D. Vanderbilt, Phys. Rev. Lett. **98**, 217602 (2007).
[29] N. A. Pertsev, A. G. Zembilglotov, and A. K. Tagantsev, Phys. Rev. Lett. **80**, 1988 (1998).
[30] Z.-G. Ban and S. P. Alpay, J. Appl. Phys. **91**, 9288 (2002).
[31] L. Bellaiche, J. Iniguez, E. Cockayne, and B. P. Burton, Phys. Rev. B **75**, 014111 (2007).